JOURNAL OF MATERIALS SCIENCE **39** (2004) 173–180

SiC/SiC minicomposites with $(PyC/TiC)_n$ interphases processed by pressure-pulsed reactive CVI

O. RAPAUD, S. JACQUES*, H. DI-MURRO, H. VINCENT, M.-P. BERTHET, J. BOUIX
Laboratoire des Multimatériaux et Interfaces—UMR 5615 CNRS/University of Lyon 1 43, boulevard du 11 Novembre 1918, Bât. Berthollet F-69622 Villeurbanne Cedex, France
E-mail: sylvain.jacques@adm.univ-lyon1.fr

(Pyrocarbon/titanium carbide)$_n$ multilayered interphases were prepared within SiC/SiC minicomposites by a new method: pressure-pulsed reactive chemical vapour infiltration (P-RCVI). This method combines P-CVI with reactive chemical vapour deposition (RCVD). Minicomposite tensile tests with unload-reload cycles have shown that the interfacial shear stress depends on the number of $TiCl_4$ gas pulses used for the processing of TiC sub-layers. TEM observations have shown, that with a few gas pulses, the carbide nucleates as isolated grain islands which disturbs the structural anisotropy of the pyrocarbon. This structure results in a good mechanical fibre/matrix load transfer. By increasing the number of gas pulses, the TiC sub-layers become continuous and it is possible to partially consume the highly ordered pyrocarbon sub-layers, but, in that case, the load transfer is poor. The specimen behaviour in air at 700°C under a constant tensile loading was assessed. Compared with a pure pyrocarbon reference interphase, the interphases containing TiC significantly improve the lifetime of the SiC/SiC minicomposites.

1. Introduction

In SiC/SiC type ceramic matrix composites (CMCs), a good toughness can be achieved if matrix cracks, which initiate in the brittle matrix during a mechanical loading, are deflected and do not penetrate the fibre reinforcement. The control of the strength of the fibre/matrix bonding allows a damageable behaviour, with a good load transfer from the matrix to the fibres, to be obtained [1, 2].

This fibre/matrix coupling can be tailored by adding, between the fibre and the matrix, a sub-micrometer thin layered film called an "interphase". Naslain *et al*. [3–5] have demonstrated that a nano-scale multilayered interphase (PyC/carbide)$_n$ composed of n alternations of pyrocarbon (PyC) and carbide sub-layers can fulfil this purpose. Thickness of sub-layers as low as a few nanometers could be obtained by using low pressure-pulsed chemical vapour infiltration (P-CVI).

In previous work in our laboratory, thin carbide (M_xC) layers were obtained on carbon substrates by reactive CVD (RCVD) [6, 7]. In this method, only the M element of the carbide is carried by the gas phase, carbon being supplied by the substrate itself after diffusion through the growing carbide layer. Hence, on the one hand, during the growth of a carbide layer by RCVD, it is possible to partially consume a previously deposited PyC sub-layer, which should reduce the air sensitivity of a (PyC/carbide)$_n$ coating. On the other hand, the carbon diffusion through the carbide allows a good adhesion of the coating, which should promote a good mechanical load transfer in CMCs.

The aim of the present work was to combine both methods (P-CVI and RCVD) in order to prepare, within 1D minicomposites, (PyC/carbide)$_n$ interphases and to characterize these minicomposites. Titanium carbide was chosen for this study because titanium reacts easily with carbon to form TiC by RCVD and because carbon can diffuse rapidly through this carbide.

2. Experimental procedure

2.1. Samples

The samples used in this study were SiC/SiC minicomposites. A minicomposite is a 1D model composite. It consists of a tow in which the interphase and then the SiC matrix are infiltrated by CVI methods. The tow is composed of around 500 Hi-Nicalon fibres (monofilaments) (from Nippon Carbon, Japan) (Fig. 1).

The geometry of the minicomposite is simpler than that of the actual composite. It can properly simulate its behaviour and, specially, enables the determination of the interphase properties [8].

Before infiltration, the sizing of the as-received Hi-Nicalon fibres was removed by a treatment of fibre

*Author to whom all correspondence should be addressed.

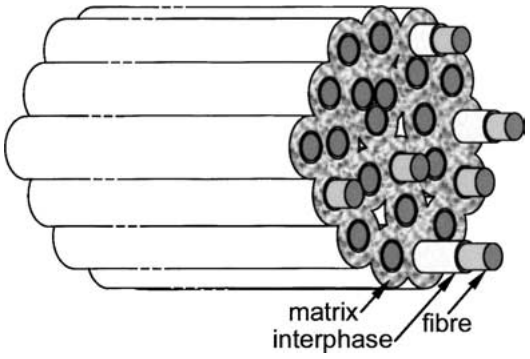

Figure 1 Schematics of a minicomposite prepared by CVI (for clarity, only a few fibres out of the 500 that constitute a whole tow are represented).

bundles at 950°C for one hour under primary vacuum. Then, the ends of 70 mm length fibre tows were attached to a graphite frame with carbon paste for infiltration of PyC and TiC sub-layers and the SiC matrix. As described in reference [9], the tows were slightly twisted (1.5 turn/70 mm) in order to reach a minicomposite fibre volume fraction of about 50% (checked by weighing). The interphases were about 0.5 μm in thickness.

2.1.1. Multilayered coatings processing

Pyrocarbon was infiltrated by P-CVI and titanium carbide was infiltrated by P-RCVI (pressure Pulsed Reactive Chemical Vapour Infiltration), which combines P-CVI and reactive CVD. Pulsed methods are based on a succession of sequences (the "pulses"), which can be broken down into three separate stages [3–5, 10, 11]:

- introduction of gas mixture into the reactor chamber during 0.5 s and thus increase of reactor pressure,
- reaction of gases with the substrate or with the previously infiltrated sub-layer for five seconds in a closed chamber,
- evacuation phase, which should be as short as possible since no reaction between gaseous species and substrate is supposed to occur during this time (fixed to four seconds).

The fibre-tow treatment apparatus included a horizontal quartz tube (30 mm inner diameter) heated by an electrical resistance furnace. The temperature was controlled with a Pt/PtRh thermocouple located between furnace heating elements. The quasi-isothermal hot area was 10 cm in length. The gaseous species were fed to the reactor and evacuated through pneumatic valves operated with an automatic control device. The reactor pressure was measured with a pressure transmitter (Keller, model PAA-21, Switzerland). A rotary vane vacuum pump was used at the outlet of the apparatus and equipped with liquid nitrogen traps. Buffer tanks were placed upstream from the furnace in order to have sufficient gas supplies at disposal for rapid peak pressure establishment within the reactor chamber. The

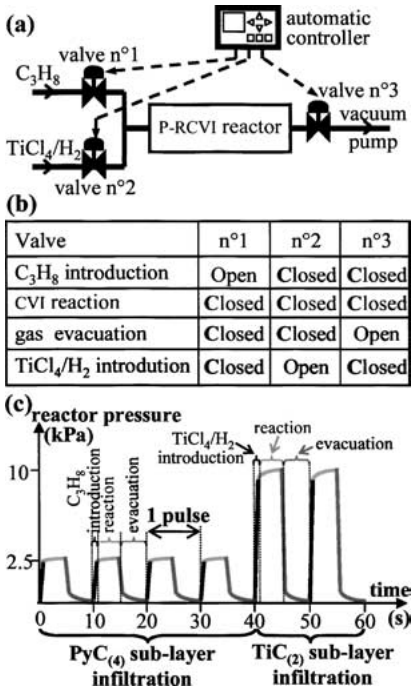

(b)

Valve	n°1	n°2	n°3
C_3H_8 introduction	Open	Closed	Closed
CVI reaction	Closed	Closed	Closed
gas evacuation	Closed	Closed	Open
$TiCl_4/H_2$ introdution	Closed	Open	Closed

Figure 2 Schematics of (a) P-RCVI apparatus, (b) valve states versus pulse CVI step, and (c) example of pulse sequence for a $(PyC_{(4)}/TiC_{(2)})_1$ bi-layer processing.

CVI apparatus, the status statement of the valves during pulse sequences as well as an example of pressure variation versus time are schematically represented in Fig. 2.

For PyC layer infiltration, propane was the gas precursor and the supply pressure was 2.5 kPa. TiC was infiltrated from a $TiCl_4/H_2$ gas mixture with a supply pressure of 10 kPa. The titanium tetrachloride vapour was carried by hydrogen through a gas bubbler. H_2 was used as both a carrier gas and a reducing agent. H_2 was provided through two lines, one going through the bubbler and a parallel one for dilution. The quantity of carried $TiCl_4$ gas was determined by H_2 flow rates, $TiCl_4$ vapour pressure at bubbler temperature (1675 Pa at 25°C) and the operating pressure within the distribution line (10 kPa). In these conditions, the reactant concentration ratio was: $[H_2]/[TiCl_4] \approx 15$.

The multilayered coatings were designated as $(PyC_{(n_p^{PyC})},TiC_{(n_p^{TiC})})_n$ where n_p^{PyC} was the number of propane pulses chosen for each PyC sublayer infiltration, n_p^{TiC} was the number of $TiCl_4/H_2$ pulses used for TiC infiltration and n was the total number of (PyC, TiC) bi-layers within the film. The example of pressure cycling given in Fig. 2c corresponds to one $(PyC_{(4)}/TiC_{(2)})_1$ bi-layer processing. Thick coatings were first infiltrated with up to several hundreds of gas pulses in order to assess the growth (and/or consumption) rates in tows. Then, three kinds of sub-micrometric multilayered interphases were prepared within minicomposites. In all cases n_p^{PyC} was fixed to 7 for each interphase pyrocarbon sub-layer. n_p^{TiC} was equal to 2 for each carbide sub-layer in the first interphase containing 40 bi-layers and denoted as $(PyC_{(7)}, TiC_{(2)})_{40}$, n_p^{TiC} was equal to 11 in the second one containing 20 bi-layers and denoted as $(PyC_{(7)},TiC_{(11)})_{20}$. n_p^{TiC} was increased from 1 to 20 (in unit steps from one carbide sub-layer

to the other) in order to obtain a third "graded" interphase denoted as ($PyC_{(7)}$, $TiC_{(n_p^{TiC})})_{20}$. For comparison, a pure pyrocabon interphase denoted as ($PyC_{(320)}$) was also prepared within fibre tows, with 320 pulses of propane.

2.1.2. SiC matrix processing

The SiC matrix was infiltrated by classical CVI in a second hot-wall reactor (50 mm in inner diameter chamber) from CH_3SiCl_3/H_2 precursor gases at 950°C. The ratio $[H_2]/[CH_3SiCl_3]$ was 4, the total gas flow rate was 250 cm^3 min^{-1} and total pressure 2 kPa. The duration of matrix infiltration was 7 h.

2.2. Characterization

2.2.1. Mechanical behaviour

The minicomposites were tensile tested at room temperature with unload-reload cycles using a MTS machine (ref Synergie 400, USA) equipped with a 2 kN load cell. The minicomposite ends were glued with an epoxy resin (Lamplan, ref 607, France) in metallic tubes separated by 40 mm that were then gripped into the testing machine jaws. The crosshead speed was 0.05 mm/min. The strain was measured with an extensometer (MTS, model 634.11F54, USA) directly gripped on the minicomposite itself. The extensometer gauge length was 25 mm. Acoustic emission measurements were used to detect the matrix cracks during minicomposite stressing. The total number of matrix cracks was verified by optical microscopy on polished longitudinal sections of the failed minicomposites after chemical etching (Murakami reactant) [12] in order to reveal the matrix microcracks which were close during unloading. The interfacial shear stress τ was estimated by the following two methods.

In the first method (called LRE) proposed by Lamon *et al.* [13] τ is calculated from hysteresis loop widths $\delta\Delta$ measured at different stress levels σ (Fig. 3).

In the second method (called ORRVF) proposed by Olivier *et al.* [14, 15] mathematical quadratic equations of unloading and reloading curves are obtained from hysteresis loop modelling. Different cases are considered depending on (among other parameters) (i) the comparison between the fibre slip zone length and the fibre/matrix debond length near the matrix crack and

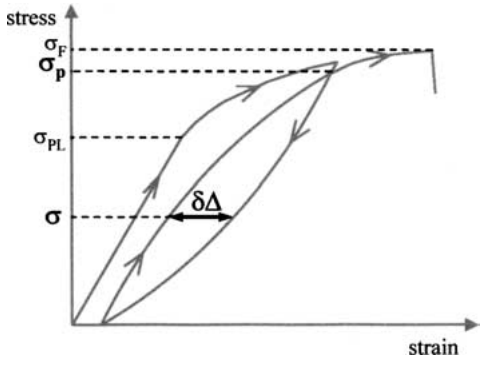

Figure 3 Schematics of minicomposite stress-strain curve with one hysteresis loop obtained from one unload-reload cycle.

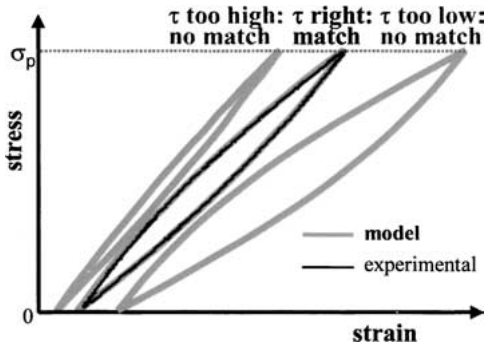

Figure 4 Example of method ORRVF computation applied to one hysteresis loop: when the right τ value is used the model curve is superimposed on the experimental unload-reload cycle.

(ii) the matrix cracking saturation. The decrease of the composite stiffness during matrix microcracking is taken into account. The procedure lies in computing model curves by varying τ until they match the experimental curves (Fig. 4). In both methods, assuming that it was constant, τ was worked out from every hysteresis loop from one specimen knowing the number of matrix cracks at the maximum stress σ_p of each cycle.

2.2.2. Oxidation tests

In order to study the oxidation resistance of the interphases, the minicomposites were submitted to thermal ageing in air under a static loading following a procedure described in reference [16]. Each specimen, with a 25 mm gauge length, was vertically maintained in the hot area of a furnace between two alumina tubes with an alumina-based adhesive (AREMCO ref. 603, USA). At each alumina rod end, hooks allowed device self-alignment. Once the temperature reached the set-point of 700°C, a load was very carefully hooked to the bottom end of the alumina tube in the cold area. In order to ensure the same degree of minicomposite damage for any interphase, the load corresponded to a force of 15 N above the average proportional limit obtained from tensile tests. The time of ageing before failure was automatically measured by means of a timer connected to a switch which stopped the timer in case of failure. The minicomposite was exposed to a dry air stream at 700°C (from the top to the bottom) obtained from liquid air evaporation.

2.2.3. Coating microstructure and texture

The morphology of the thick-graded multilayered coating fracture surfaces was observed with a scanning electron microscope (SEM) (HITACHI S800).

Thin longitudinal sections of minicomposites after tensile test were studied by transmission electron microscopy (TEM: TOPCON 002B, Japan) using bright-field, high resolution (HR) and selected area diffraction (SAD) techniques. The samples were embedded in a ceramic cement (CERAMABOND 503, Aremco Products Inc., USA) and mechanically thinned. The thin sheets (~60 μm in thickness) were then ion-milled (GATAN PIPS, USA) to electron transparency.

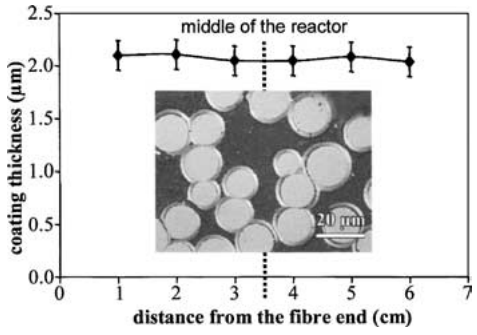

Figure 5 Mean values of ($PyC_{(1000)}$) coating thickness along the fibre tow and optical microscopy observation of a polished cross section (insert).

3. Results

3.1. Thick coatings

3.1.1. Infiltration of pyrocarbon by P-CVI

Mean values of ($PyC_{(1000)}$) coating thickness obtained from numerous microscopic observations are reported in Fig. 5. The pyrocarbon deposit is homogeneous along and within the fibre tow. The average pyrocarbon deposition rate is 2.15 nm/pulse.

3.1.2. Infiltration of titanium carbide by P-RCVI

In order to study the infiltration and the growth of TiC, a thick-graded multilayered coating has been processed. In this case, the sequence is ($PyC_{(200)}$/$TiC_{(n_p^{TiC})}$)$_4$ + ($PyC_{(200)}$): a constant number of pulses for each pyrocarbon layer infiltration ($n_p^{PyC} = 200$) has been used, while a progressive one has been used for TiC layer deposits ($n_p^{TiC} = 50$, 100, 150 and 200). An additional ($PyC_{(200)}$) sub-layer has been infiltrated. The coating is homogeneous too and present around every fibre when it is separated enough from the others to permit gas infiltration (Fig. 6).SEM observation enables an indentity of each sub-layer and a measure of the size evolution (Fig. 7). As n_p^{TiC} and TiC layer thickness are increasing together, PyC thickness is decreasing owing to the carbon consumption occurring during the P-RCVI carbide growth. When extrapolating TiC thickness to zero, the curve starts at $n_p^{TiC} \approx 30$ instead of zero. This feature seems to emphasize the existence of an initial CVI step occurring prior to thick TiC layer growth.

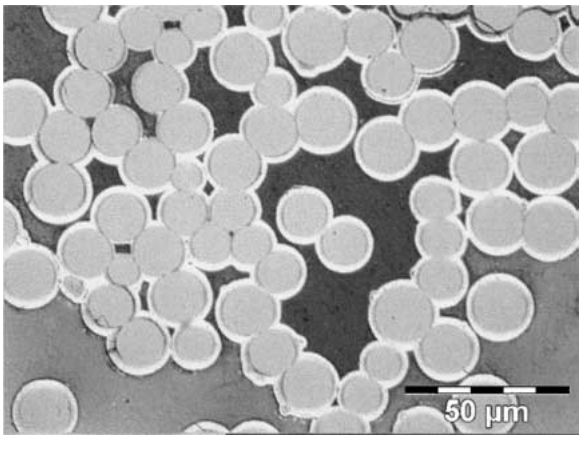

Figure 6 Optical microscopy observation of a polished cross section of a fibre tow infiltrated by a thick-graded multilayered coating: ($PyC_{(200)}$/$TiC_{(n_p^{TiC})}$)$_4$ + ($PyC_{(200)}$) with $n_p^{TiC} = 50$, 100, 150, 200.

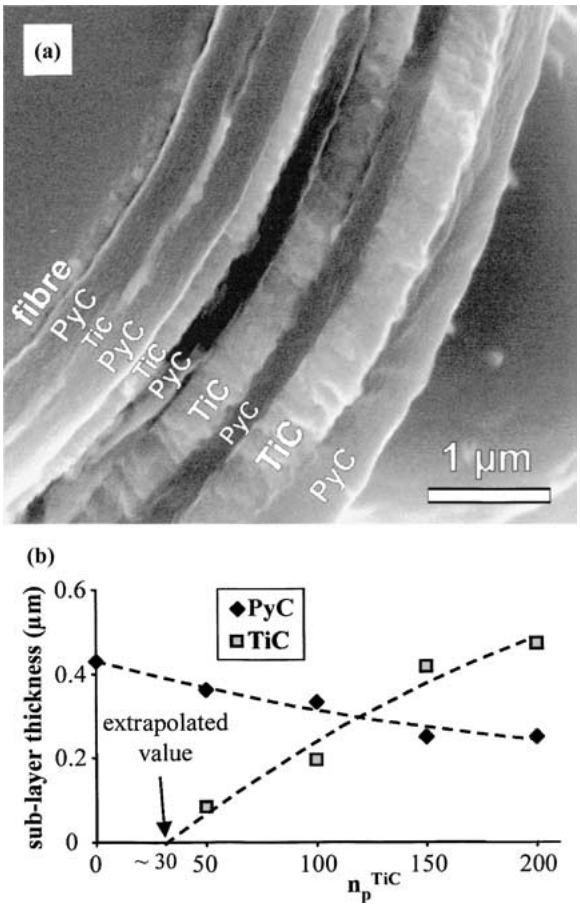

Figure 7 SEM observation of the thick-graded multilayered coating ($PyC_{(200)}$/$TiC_{(n_p^{TiC})}$)$_4$ + ($PyC_{(200)}$) (a) and sub-layer thickness versus n_p^{TiC} (b).

3.1.3. SiC matrix infiltration by low pressure CVI

Optical microscopy observation of a reference SiC/SiC minicomposite (Fig. 8) reveals that the matrix infiltration is homogeneous. In this case, the fibre volume fraction is 35%.

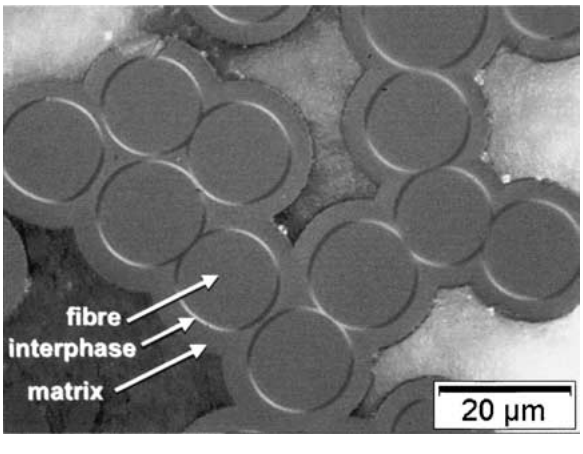

Figure 8 Optical microscopy observation in polarized light of a polished cross section of a reference minicomposite.

TABLE I Average tensile mechanical characteristics of each batch of minicomposites and interfacial shear stresses τ obtained from methods LRE and ORRVF. ε_{PL} and F_{PL} are the proportional limit strain and force, ε_F and F_F are the strain and force at failure. N is the total number of matrix cracks measured from acoustic emission and V_f the volume fraction of fibres

Interphase	ε_{PL} (%)	F_{PL} (N)	ε_F (%)	F_F (N)	N	V_f (%)	τ_{LRE} (MPa)	τ_{ORRVF} (MPa)
$PyC_{(320)}$ (reference)	0.08	54	0.44	98	654	35	45	45
$(PyC_{(7)}/TiC_{(2)})_{40}$	0.14	80	0.79	193	689	46	155	400
$(PyC_{(7)}/TiC_{(11)})_{20}$	0.16	66	0.60	138	1822	54	90	155
$(PyC_{(7)}/TiC_{(n_p^{TiC})})_{20}$[a]	0.17	72	0.94	189	1030	50	55	110

[a]Graded interphase with $n_p^{TiC} = 1, 2, \ldots, 20$.

3.2. Minicomposite interphases

3.2.1. Mechanical behaviour

Average tensile mechanical characteristics at ambient temperature for the four batches of minicomposites are presented in Table I. Fig. 9 displays a typical force-strain curve for each kind of interphase. In every case, an extended non-linear domain evidencing matrix microcracking and fibre/matrix debonding follows the initial linear elastic region. Therefore, the four kinds of interphase act as mechanical fuses.

The best mechanical properties are achieved with interphase $(PyC_{(7)}/TiC_{(2)})_{40}$ and with the graded interphase. However, the latter exhibits broader loops and a pronounced plateau-like feature followed by a change of slope at matrix crack saturation. This feature is evidence for a relatively poor fibre/matrix load transfer. The weakest properties are obtained with interphase $(PyC_{(7)}/TiC_{(11)})_{20}$ and specially with the reference ($PyC_{(320)}$) interphase.

Despite the differences arising from the two methods used for τ evaluation, the trend obtained for interfacial shear stress confirms the observed mechanical behaviour; intercalating TiC in the pyrocarbon interphase results in a strengthening of the fibre/matrix bonding. However, the best fibre/matrix load transfer is obtained when a restricted number of gas pulses is used. Thus, increasing n_p^{TiC} (as in interphase $(PyC_{(7)}/TiC_{(11)})_{20}$ or in the graded interphase) decreases τ, but the interfacial shear stress remains higher than the reference one.

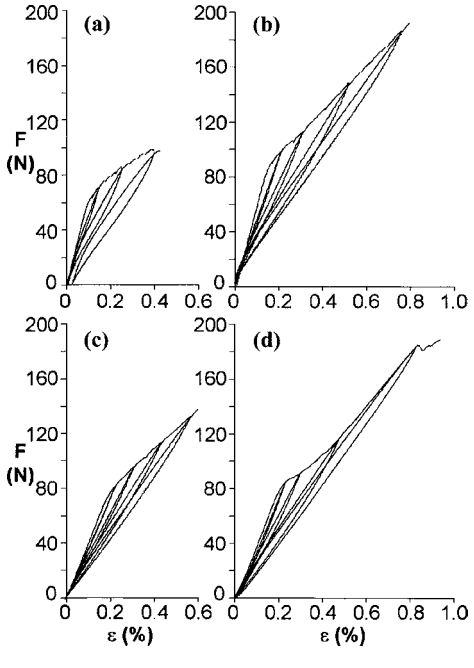

Figure 9 Tensile force-strain curves with unload-reload cycles for minicomposites with reference interphase $PyC_{(320)}$ (a), interphase $(PyC_{(7)}/TiC_{(2)})_{40}$ (b), interphase $(PyC_{(7)}/TiC_{(11)})_{20}$ (c) and graded interphase $(PyC_{(7)}/TiC_{(n_p^{TiC})})_{20}$ where $n_p^{TiC} = 1, 2, 3 \ldots 20$ (d) (for clarity only a few hysteresis loops are represented).

3.2.2. TEM characterization

TEM observation of the interfacial area in a minicomposite with the graded interphase $(PyC_{(7)}/TiC_{(n_p^{TiC})})_{20}$ ($n_p^{TiC} = 1, 2, 3, \ldots, 20$) shows that the multilayered coating infiltration has been homogeneous within the specimen (Fig. 10). In Fig. 10a, the SiC matrix infiltrated between 1 μm apart fibres can be observed. The (PyC/TiC) sequences are visible within the interphase (Fig. 10b), the sub-layers are continuous and well separated. However, only about a dozen out of the expected twenty TiC sub-layers are visible in this observed area.

The very first TiC sub-layers deposited against the fibre with low numbers of pulses ($n_p^{TiC} < 8$) seem to be absent. Instead of them, a thick pyrocarbon sub-layer is observed in HR mode (Fig. 10e) with poorly orientated (002) lattice fringes. Nevertheless, some isolated TiC grain islands could be observed within the pyrocarbon layer near the fibre but in other areas of the thin foil.

When n_p^{TiC} increases, the thickness of the TiC sub-layers increases up to 15 nm for $n_p^{TiC} = 20$ while the thickness of the PyC sub-layers decreases because of carbon consumption during P-RCVI. The pyrocarbon intercalated between two TiC sub-layers in this n_p^{TiC} range ($8 < n_p^{TiC} < 20$) is well organised, the (002) atomic layers are stacked parallel to each other (Fig. 10d). Near the matrix (when n_p^{TiC} reaches 20), some (002) carbon planes are remaining between the carbide sub-layers (Fig. 10c).

The whole interphase SAD pattern shows the turbostratic pyrocarbon (002) arcs with a rather low arc-opening angle due to the average structural anisotropy. The other present diffraction spots are characteristic of nano-crystallised titanium carbide.

3.3. Ageing at high temperature under tensile loading

The minicomposite ageing times at 700°C in dry air under load are reported in Table II. The minicomposite with pure PyC reference interphase broke after 20 h. This result proves carbon sensitivity toward oxidation. For the minicomposites with interphases containing TiC, the lifetimes are significantly improved: the experiments were stopped before specimen failure

TABLE II Minicomposite ageing times at 700°C in dry air under load

Interphase	Load (kg)	Lifetime (h)
$PyC_{(320)}$ (reference)	7	20 (failure)
$(PyC_{(7)}/TiC_{(2)})_{40}$	9.5	>115
$(PyC_{(7)}/TiC_{(11)})_{20}$	8.5	>300
$(PyC_{(7)}/TiC_{(n_p^{TiC})})_{20}$[a]	9	>300

[a]Graded interphase with $n_p^{TiC} = 1, 2, \ldots, 20$.

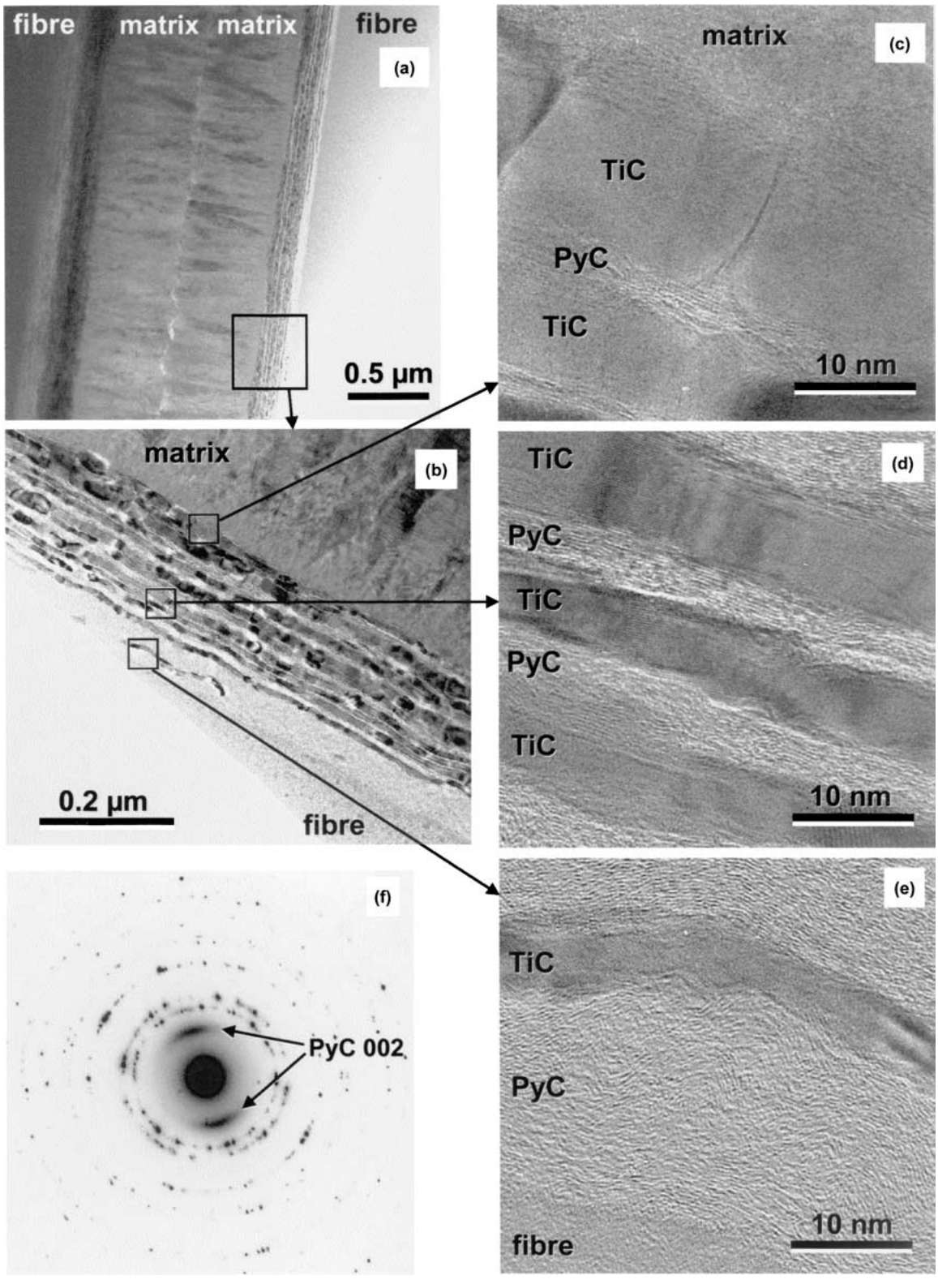

Figure 10 TEM observation of a SiC/$(PyC_{(7)}/TiC_{(n_p^{TiC})})_{20}$/SiC minicomposite with $1 \leq n_p^{TiC} \leq 20$ according to the Bright Field mode (a) and (b), to the High Resolution mode (c), (d) and (e) and interphase SAD pattern (negative) (f).

after 115 h with interphase $(PyC_{(7)}/TiC_{(2)})_{40}$ and even after 300 h with the others.

4. Discussion

4.1. Relation between structures of fibre/matrix interfaces and minicomposite mechanical behaviour

The multilayered interphases were processed with $n_p^{TiC} \leq 20$, i.e., during the initial step for TiC CVI growth as emphasized by the kinetic study (Fig. 7). This step is characterised by localized carbide grain nucleation occurring at a small number of gas pulses ($n_p^{TiC} < \sim 8$) which disturbs the pyrocarbon orientation. This structure should promote intense friction and restrict fibre sliding in the matrix sheath during unload-reload cycles. The result is a strong fibre/matrix bonding as evidenced by interfacial shear stress values; up to 400 MPa as measured with method ORRVF and

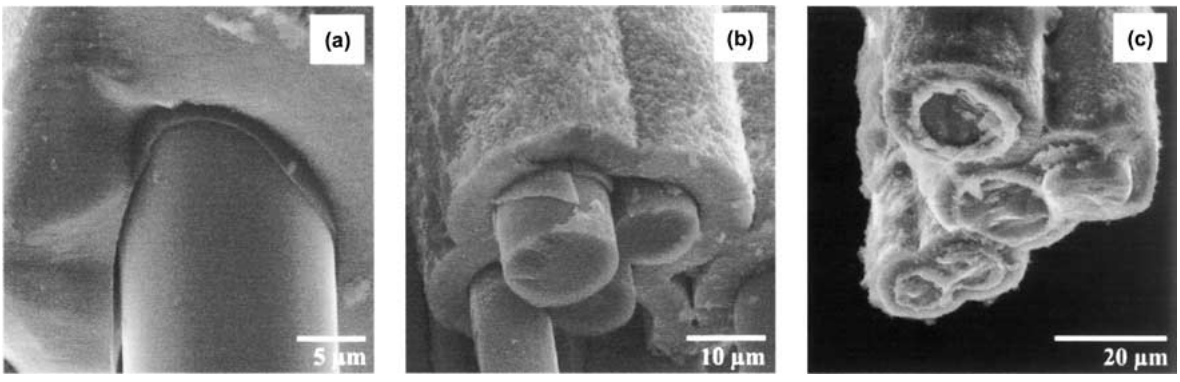

Figure 11 SEM observation of minicomposites after ageing under load with reference interphase $PyC_{(320)}$ (a), interphase $(PyC_{(7)}/TiC_{(2)})_{40}$ (b) and interphase $(PyC_{(7)}/TiC_{(11)})_{20}$ (c).

155 MPa with method LRE. It is worth noting that the difference between these values lies in the measurement of only the hysteresis loop width with method LRE but also of the global cycle shape (linear or quadratic aspect, slope, residual strain. . .) in method ORRVF. Thus, although both methods are based on models which use the same original hypotheses [13–15, 17–23], the latter seems more reliable. Nevertheless, the former has the merit of being less tedious to run and allows a rapid identity of a trend from one specimen to the other.

When the number of $TiCl_4/H_2$ gas pulses is higher ($8 \leq n_p^{TiC} \leq 20$), the high turbostratic carbon ordering and the smooth continuous carbide sub-layer promote the deflection of matrix cracks from mode I to mode II over long distances along the interfaces. More extensive sliding can occur between sub-layers and the resulting τ is lower. For the graded interphase processed by increasing n_p^{TiC} from one sub-layer to the other, the resulting interfacial shear stress is also low, which indicates that the crack deflection occurs mainly in the "weakest link" of this interphase (i.e., in the part made with $n_p^{TiC} > 8$).

4.2. Ageing under load

The lifetime improvement observed with interphases containing carbide is surprising because TiC is not known to be oxidation resistant [24]. On the one hand in the case of interphase $(PyC_{(7)}/TiC_{(2)})_{40}$, the interfacial coating morphology does not seem to be altered despite the low carbide proportion (Fig. 11b). This result might be explained by the good fibre/matrix load transfer, which restricts the crack opening and thus the access of oxidising atmosphere to the interphase. Conversely, the morphology of interphase $(PyC_{(7)}/TiC_{(11)})_{20}$, which contains more carbide, has changed during ageing probably because of oxide formation (Fig. 11c). In that case, the lowest interfacial shear stress and greater crack-opening displacement results in ease of gaseous penetration to the interphase. Further investigation is in progress in order to understand the phenomena involved during these ageing tests.

5. Conclusions

$(PyC/TiC)_n$ multilayered coatings have been prepared by P-RCVI. The homogeneity of infiltration is good within Hi-Nicalon fibre tows. In the case of thick coatings infiltrated with several hundreds of gas pulses, pyrocarbon consumption and carbide growth have been measured by SEM. An initiation growth step has been evidenced for $n_p^{TiC} < 30$.

Nano-scale multilayered coatings have been processed as interphases in SiC/SiC minicomposites. When $n_p^{TiC} < 8$, a nucleation of isolated TiC grain islands occurs which disturbs the pyrocarbon orientation; the result is a strong fibre/matrix bonding and a good mechanical transfer. When $8 \leq n_p^{TiC} \leq 20$, smooth continuous carbide sub-layers and a high pyrocarbon structural anisotropy are observed by TEM; the result is a global poor fibre/matrix bonding as shown by interfacial shear stress measurements.

Finally, compared with pure pyrocarbon interphase, the lifetimes of minicomposites with $(PyC/TiC)_n$ interphases at 700°C in air under load are improved.

Acknowledgements

The authors are grateful to D. Rouby from GEMPPM (INSA-Lyon in France) for loan of an acoustic emission device and for fruitful discussions.

References

1. R. NASLAIN, *Comp. Inter.* **1** (1983) 253.
2. A. G. EVANS and F. W. ZOK, *J. Mater. Sci.* **29** (1994) 3857.
3. R. NASLAIN, *Solid State Ionics* **141/142** (2001) 541.
4. F. HEURTEVENT, PhD thesis no. 1476, University of Bordeaux-1, Bordeaux, France, 1996.
5. S. BERTRAND, O. BOIRON, R. PAILLER, J. LAMON and R. NASLAIN, in "High Temperature Ceramic Matrix Composites III," edited by K. Niihara, K. Nakano, T. Sekino and E. Yasuda (Key Engineering Materials, 1999) Vols. 164/165, p. 357.
6. J. BOUIX, C. VINCENT, H. VINCENT and R. FAVRE, *Mater. Res. Soc.* **168** (1990) 305.
7. J. BOUIX, M. P. BERTHET, F. BOSSELET, R. FAVRE, M. PERONNET, O. RAPAUD, J. C. VIALA, C. VINCENT and H. VINCENT, *Comp. Sci. Technol.* **61** (2001) 355.
8. R. NASLAIN, J. LAMON, R. PAILLER, X. BOURRAT, A. GUETTE and F. LANGLAIS, *Composites-Part A (Appl. Sci. Manufact.)* **30A** (1999) 537.
9. S. BERTRAND, P. FORIO, R. PAILLER and J. LAMON, *J. Amer. Ceram. Soc.* **82** (1999) 2465.
10. P. DUPEL, R. PAILLER, X. BOURRAT and R. NASLAIN, *J. Mater. Sci.* **29** (1994) 1056.
11. P. DUPEL, X. BOURRAT and R. PAILLER, *Carbon* **33** (1995) 1193.

12. V. CARLE, U. SCHÄFER, U. TÄFFNER, F. PREDEL, R. TELLE and G. PETZOW, *Pract. Met.* **28** (1991) 359.
13. J. LAMON, F. REBILLAT and A. G. EVANS, *J. Amer. Ceram. Soc.* **78** (1995) 401.
14. C. OLIVIER, PhD thesis no. 1998ISAL0035, INSA-Lyon, France, 1998.
15. C. OLIVIER, P. REYNAUD, D. ROUBY, J. B. VEYRET and G. FANTOZZI, *Sil. Ind.* **63** (1998) 137.
16. S. JACQUES, A. LOPEZ-MARURE, C. VINCENT, H. VINCENT and J. BOUIX, *J. Europ. Ceram. Soc.* **20** (2000) 1929.
17. D. B. MARSHALL and W. C. OLIVER, *J. Amer. Ceram. Soc.* **70** (1987) 542.
18. P. G. CHARALAMBIDES and A. G. EVANS, *ibid.* **72** (1989) 746.
19. J. W. HUTCHINSON and H. JENSEN, *Mech. Mater.* **9** (1990) 139.
20. W. A. CURTIN, *J. Amer. Ceram. Soc.* **74** (1991) 2837.
21. D. B. MARSHALL, *Acta. Metall. Mater.* **40** (1992) 427.
22. M. Y. HE, X. WU, A. G. EVANS and J. W. HUTCHINSON, *Mech. Mater.* **18** (1994) 213.
23. E. VAGAGGINI, J. M. DOMERGUE and A. G. EVANS, *J. Amer. Ceram. Soc.* **78** (1995) 2709.
24. S. SHIMADA, *J. Mater. Sci.* **31** (1996) 673.

Received 29 January
and accepted 25 August 2003